Appl. Phys. B 92, 25–32 (2008)
DOI: 10.1007/s00340-008-3063-x

Applied Physics B
Lasers and Optics

J. GAGNON[1,✉]
E. GOULIELMAKIS[1]
V.S. YAKOVLEV[2]

The accurate FROG characterization of attosecond pulses from streaking measurements

[1] Max Planck Institute für Quantenoptik, Hans-Kopfermann-Straße 1, 85748 Garching, Germany
[2] Ludwig Maximilians Universität, 85748 Garching, Germany

Received: 20 May 2008
Published online: 10 June 2008 • © The Author(s) 2008

ABSTRACT We describe a new attosecond FROG algorithm optimized for the characterization of sub-100 as pulses from streaked electron spectra. We make improvements upon the treatment of the attosecond streaking spectrogram, and show that these are necessary in order to accurately characterize shorter pulses with ever larger bandwidths. We investigate the effects of the approximations that must be made in order to apply the generalized projections scheme.

PACS 31.15.xg; 32.90.+a; 33.60.+q

1 Introduction

The ability to probe physical events on an unprecedented timescale, the attosecond scale, has brought with it new challenges. Namely, the task of extracting information beyond just the duration of physical processes is essential for a deeper understanding of the physics of atoms and molecules, and for the verification of theoretical predictions. The photoionization by an attosecond light pulse, Auger decay, tunnelling ionization [1], shake-up, or a combination of these, may result in the emission of electron wave packets within an attosecond time interval. The attosecond streaking measurement [2, 3] is a powerful technique which has proven to be effective in extracting information about the temporal character of attosecond electron emissions [4, 5].

Moreover, attosecond streaking has been shown to provide a complete characterization of attosecond light pulses [6] by borrowing principles behind frequency-resolved optical gating (FROG). The attosecond version of FROG, known as FROG CRAB, has successfully been used to characterize ~ 130 as pulses [7]. We developed a FROG retrieval algorithm which is optimized for attosecond streaking, and provides a more reliable and accurate characterization of attosecond pulses. We demonstrate that our method is crucial for processing spectrograms recorded under realistic experimental conditions, and is especially suitable for the characterization of attosecond pulses approaching the single cycle limit. Furthermore, we improve the treatment and investigate the effects of the approximations that must be made in order to apply the attosecond FROG retrieval, and establish the parameter range for which it can be used.

✉ Fax: +49-89-32905649, E-mail: justin.gagnon@mpq.mpg.de

2 Basic principles

We consider a class of attosecond measurements where an XUV pulse photoionizes atoms in the presence of an infrared (IR) laser field [8, 9]. The energy distribution of the outgoing electrons contains information about the XUV pulse. Without the influence of the laser field, only the spectrum of the XUV pulse can be measured, not its temporal profile. The interaction of the laser field with the emerging electron wave packet encodes the time structure of the IR and XUV fields into the photoelectron spectrum. This approach has been dubbed the "attosecond streak camera" [9], where streaking is defined as the laser-dressed emission of electron wave packets. The characterization of attosecond pulses can be achieved by measuring streaked electron spectra at different delays between the XUV pulse and a controlled laser field, also referred to as a streaking field. Under the single active electron approximation, the momentum-space continuum wave function of electrons photoionized by XUV pulses under the influence of a time-delayed infrared (IR) streaking laser pulse can be expressed as [9–11]

$$\Phi(p,\tau) = \int_{-\infty}^{\infty} E_X(t) d(p + A_L(t+\tau)) e^{-i\varphi(p,t+\tau)} e^{i(p^2/2 - \Omega_X + W)t}\, dt\,, \tag{1}$$

$$\varphi(p,t) = \int_{t}^{\infty} \left(pA_L(t') + \frac{1}{2}A_L^2(t') \right) dt'\,. \tag{2}$$

In these expressions, p is the final momentum of the electron in the continuum, Ω_X is the central XUV photon energy, W is the ionization potential of the atom, τ is the delay between the XUV and IR pulses, A_L is the vector potential of the IR pulse, $d(p)$ is the dipole transition matrix element between the initial ground state and continuum state with momentum p, $E_X(t)$ represents the complex valued envelope of the XUV pulse, and $\varphi(p,t)$ is the quantum phase shift that the electron acquires due to its interaction with the laser field, from the mo-

ment of ionization until it reaches the detector. Expressions (1) and (2) are given in atomic units, which are used throughout this paper.

A record of streaked electron spectra, $\tilde{S}(p,\tau) = |\Phi(p,\tau)|^2$, taken at different delays τ between the XUV and IR fields, models a spectrogram acquired in a streaking measurement. From such a measurement, it is possible to retrieve both the electric field of the XUV pulses [3] and the laser pulse [2]. A powerful method to accomplish this retrieval is the FROG algorithm [6]. However, further approximations must be made to apply this approach.

A FROG spectrogram is constructed according to the prescription

$$\tilde{S}(\omega,\tau) = \left| \int_{-\infty}^{\infty} P(t)G(t+\tau)\mathrm{e}^{\mathrm{i}\omega t}\,\mathrm{d}t \right|^2 , \tag{3}$$

where $P(t)$ and $G(t)$ are complex valued functions representing the pulse and gate, and τ defines a delay between them. In order to process an attosecond streaking spectrogram with a generalized projections algorithm, there cannot be inseparable terms inside the integrand of (1) that depend both on momentum and time. An inspection of (1) reveals two such terms: $d(p + A_\mathrm{L}(t))$ and $\varphi(p,t)$. We remove the momentum dependence of these terms by making the substitution $p \to p_0$, where p_0 is the central momentum of the unstreaked electrons. The effects of this central momentum approximation will be clarified later in the paper. In order to minimize the error introduced by substituting p with p_0 in the dipole transition matrix element, we first divide each measured spectrum by $|d(p)|^2$ before processing the spectrogram. As a result, the modified attosecond streaking spectrogram fed to the reconstruction algorithm is given by the following expression

$$\hat{S}(p,\tau) = \frac{|\Phi(p,\tau)|^2}{|d(p)|^2} \approx \left| \int_{-\infty}^{\infty} E_X(t)G(t+\tau)\mathrm{e}^{\frac{\mathrm{i}}{2}p^2 t}\,\mathrm{d}t \right|^2 , \tag{4}$$

$$G(t) = \frac{d(p_0 + A_\mathrm{L}(t))}{d(p_0)} \mathrm{e}^{-\mathrm{i}\int_t^\infty \left(p_0 A_\mathrm{L}(t') + \frac{1}{2}A_\mathrm{L}^2(t')\right)\mathrm{d}t'} . \tag{5}$$

This ensures that the sequence of streaked electron spectra forms a proper spectrogram as defined by (3), the XUV pulse $E_X(t)$ being gated by a function $G(t)$ that incorporates the vector potential $A_\mathrm{L}(t)$ of the laser pulse. Of particular note, when the streaking field is absent, (5) shows that the gate function $G(t)$ is unity and $\hat{S}(p,\tau)$ is just the spectrum of the XUV pulse. Thus, the retrieval of the XUV field amounts to characterizing its spectral phase, since the field-free spectrum can be measured independently.

3 Algorithm details

Having established that a record of streaked spectra (4) taken at different delays constitutes a spectrogram as defined by (3), such a spectrogram can be processed using almost exactly the same inversion tools that are used in FROG. The basic loop of the generalized projections algorithm is shown in Fig. 1. In a nutshell, a signal matrix S is computed from a pair of discretized pulse and gate vectors (step 1). The

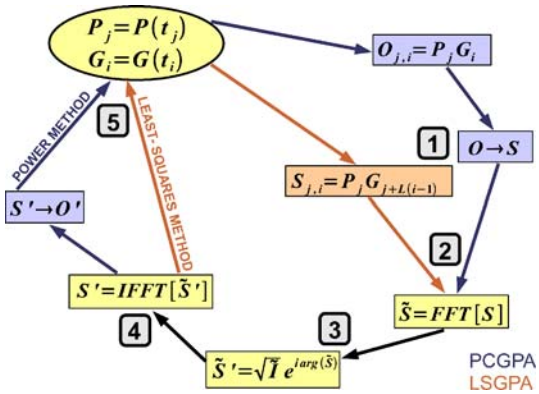

FIGURE 1 Generalized projections algorithms converge to the correct pulse and gate by applying alternating constraints between the frequency domain and the time domain. The frequency domain constraint consists of replacing the current spectral intensity with the measured one (step 3), while the minimization step (step 5) implements a time domain constraint, whereby the signal matrix is forced to have the form given by (3). Operations that are common to both the LSGPA and the PCGPA are highlighted in yellow, whereas those specific to the PCGPA are in blue, and those specific to the LSGPA are in orange

columns of this signal matrix correspond to the temporal profile of the composite signal resulting from a particular delay between the pulse and the gate. A complex spectrogram $\tilde{S}$ is obtained by Fourier-transforming the columns of S (step 2). A crucial part of the algorithm is the substitution of the modulus of $\tilde{S}$ by the square root of the measured spectral intensity $\tilde{I}$ (step 3), thereby enforcing a frequency-domain constraint on the spectrogram. The complex spectrogram $\tilde{S}'$ resulting from this operation is then inverse-Fourier-transformed back into the time domain as a signal matrix S' (step 4). Last but not least is the problem of finding the next pulse and gate pair that produce a signal matrix which most closely resembles S' (step 5). This last step can be viewed as a constraint in its own right, in the sense that the retrieved spectrogram must have the form given by (3).

The procedure of applying alternating constraints between the time and the frequency domain is known in the jargon of image processing as a "generalized projection." A particularly elegant implementation of generalized projections – and the one that was recently extended to attosecond streaking [6] for the characterization of 130 as pulses [7] – is the PCGPA [12]. In this algorithm, an outer product matrix $O_{j,i} = P_j G_i$ is first computed from a pair of discretized pulse and gate vectors, $P_j = P(t_j)$ and $G_i = G(t_i)$. The outer product matrix can then be transformed into a signal matrix by performing a row-shifting operation on it. Hence, the spectrogram can be directly related to the outer product between the pulse and gate. This framework allows for an elegant scheme, involving the power method, to extract the principal eigenvectors of $OO^\dagger$ and $O^\dagger O$, which are taken as the pulse and gate pair for the subsequent iteration (step 5 in Fig. 1). Unfortunately, the row-shifting operations assume periodic boundary conditions for the gate. If the gate is compact in time, this assumption is entirely justified. However, in the case of attosecond streaking spectrograms, (4) clearly shows that the gate function $G(t)$ does not drop to zero and generally is not periodic over the delay range of the spectrogram. Rather, the modulus of the gate $d(p_0 + A_\mathrm{L}(t))/d(p_0)$ tends to unity at extreme delays, where

the laser pulse's vector potential drops to zero. An attosecond streaking spectrogram computed using the outer product matrix formalism results in discontinuities between certain elements in the signal matrix. These discontinuities create artifacts in the calculated spectrogram, and can even hamper convergence if the spectrogram's delay boundaries are not periodic.

Furthermore, the PCGPA requires the spectrogram to be rasterized on a rectangular grid with at least as many columns as rows. In addition, the energy and delay resolutions of the spectrogram must satisfy the sampling constraint $\delta\varepsilon\delta\tau = 2\pi/N$; where N, a power of two, is the number of spectral points, and $\delta\varepsilon$ and $\delta\tau$ are respectively the energy and delay steps expressed in mutually commensurate units. As most raw experimental FROG spectrograms do not satisfy this sampling relationship, the common practice is to interpolate the measured spectrogram to produce a re-sampled version for the algorithm to work on. For a typical streaking range of 70 eV, this implies a delay step of $\delta\tau \sim 60$ as, which may be experimentally impractical. To speed up the acquisition time and to minimize the drift of experimental conditions, spectra are typically recorded at larger delay intervals. In order to satisfy the aforementioned energy-time sampling constraint, attosecond streaking spectrograms must therefore be interpolated along the delay axis prior to being fed to the retrieval algorithm.

Interpolation along the delay axis is detrimental due to the fact that the spectrogram may exhibit features that can change rapidly with respect to the delay (notably the fringe patterns resulting from the spectral interference of twin attosecond pulses, which will be discussed later on). Most importantly, the interpolation along the delay axis hinders the accurate retrieval of ever shorter attosecond pulses. As shorter attosecond pulses possess a broader bandwidth, they require a larger energy range to record a spectrogram, which leads to a finer time step (a consequence of the sampling requirement of the discrete Fourier transform). Since the PCGPA and other FROG retrieval algorithms consider the delay step to be the same as the time step, they require the spectrogram to be more heavily interpolated along the delay axis for shorter XUV pulses. Hence, current FROG algorithms inevitably lose accuracy when retrieving shorter XUV pulses.

Our implementation of generalized projections retains the robustness of other FROG retrieval algorithms, but obviates the need to interpolate the spectrogram along the delay axis, nor does it assume periodic boundary conditions for the gate. We begin by defining the elements of the signal matrix as

$$S_{j,i} = P_j G_{j+L(i-1)}\,, \quad i = 1...N_\tau\,, \quad j = 1...N_\varepsilon\,, \tag{6}$$

where N_ε and N_τ are respectively the number of energy and delay points in the spectrogram, and L is the number of time samples per delay step. This version of the signal matrix is illustrated in Fig. 2 The inclusion of the parameter L results in a much weaker sampling relation between energy and delay, $\delta\varepsilon\delta\tau = 2\pi L/N_\varepsilon$, and it greatly relaxes the constraint on the grid format of the spectrogram. Interpolation of the spectrogram along the delay axis can be avoided provided that two conditions are met:

- The spectrogram must be recorded with a uniform delay step because the signal matrix defined by (6) assumes that the number of time samples separating each spectrum is the same. However, the LSGPA can be straightforwardly adapted to incorporate variable delay steps by considering a parameter L that depends on the delay.
- The XUV field must not be confined to a time interval shorter than the delay step. Otherwise, the pulse overlaps with disconnected sections of the gate at each delay, and different arbitrary phases can be added to each of these sections without changing the spectrogram. In this case, there exists an infinite number of pulse-gate solutions to the spectrogram.

If these conditions are met, then interpolation along the delay axis can be avoided. The only remaining preprocessing consists of interpolation along the energy axis to ensure that L is an integer (i.e., an integer number of time samples must fit into the delay step) and that the number of energy points

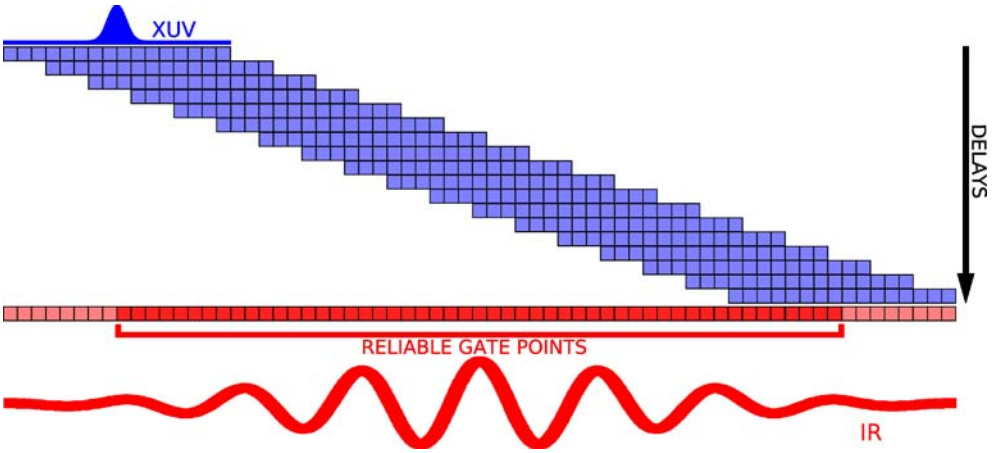

FIGURE 2 The signal matrix is constructed using the discretely sampled pulse and gate. In this example $L = 3$, and there are $N_\tau = 18$ delay values between the XUV and IR fields. The pulse is sampled with $N_\varepsilon = 16$ points, and the gate is sampled with $N_g = N_\varepsilon + L(N_\tau - 1) = 67$ points. The columns of the signal matrix are the product of the pulse and gate points for each delay. The signal matrix is therefore constructed by translating the pulse over the gate, from the most negative to the most positive delay. Since the gate is not assumed to satisfy periodic boundary conditions, it is necessarily represented over a larger temporal range than that used in the spectrogram. If the XUV pulse is compact in time, the gate points located near the extremities never interact with a substantial part of the pulse, and consequently become ill-defined

N_ε is a power of two, a prerequisite for the radix-2 FFT. By avoiding interpolating the spectrogram along the delay axis, the LSGPA does not suffer from a loss of accuracy when retrieving shorter pulses, and is therefore more suitable for accurately time-resolving attosecond processes.

By defining the signal matrix according to (6), an appropriate scheme must be used to find the best pulse and gate pair for the next iteration. Other FROG algorithms use various types of optimization strategies for performing this task. These include the downhill simplex scheme [13], and the power method for executing the singular-value decomposition in the case of the PCGPA [12]. Another standard approach we found to be particularly suitable for our definition of the signal matrix relies on the least-squares method: in order to find the next pulse P and gate G that can best reproduce the signal matrix S following the application of the spectral intensity constraint, we define a figure of merit

$$M = \sum_{i=1}^{N_\tau} \sum_{j=1}^{N_\varepsilon} \left| P_j G_{j+L(i-1)} - S_{j,i} \right|^2 . \tag{7}$$

By parameterizing the pulse and gate points either in terms of their real and imaginary parts, or by their moduli and phases, the least-squares method can be carried out, leading to the following set of equations:

$$P_j = \frac{\sum_m S_{j,m} G^*_{j+L(m-1)}}{\sum_m \left| G_{j+L(m-1)} \right|^2} , \tag{8}$$

$$G_k = \frac{\sum_n S_{k-L(n-1),n} P^*_{k-L(n-1)}}{\sum_n \left| P_{k-L(n-1)} \right|^2} , \tag{9}$$

with

$$j = 1 \ldots N_\varepsilon ,\ k = 1 \ldots N_\varepsilon + L(N_\tau - 1) ,$$

$$m = \mathrm{Max}\left(1, \left\lceil \frac{R-j+1}{L} \right\rceil + 1\right) \ldots \mathrm{Min}\left(N_\tau, \left\lceil \frac{R-j}{L} \right\rceil + N_\tau\right) ,$$

$$n = \mathrm{Max}\left(1, \left\lceil \frac{k-N_\varepsilon}{L} \right\rceil + 1\right) \ldots \mathrm{Min}\left(N_\tau, \left\lceil \frac{k}{L} \right\rceil\right) .$$

Although this system of nonlinear equations can be solved iteratively, we found that a single iteration is sufficient: a good approximate solution can be found by feeding the current gate into (8) and then using the updated pulse in (9) to obtain the new gate. This produces a pulse and gate pair that roughly minimizes the merit function M given by (7).

Now if the pulse is compact in the time domain, then Fig. 2 demonstrates that elements of the gate vector located at extreme time values never overlap with significant parts of the pulse. Since the signal matrix only provides reliable information about gate samples that overlap with sufficiently intense portions of the pulse, information about these extreme gate points is virtually absent from the signal matrix, and therefore the spectrogram. These values of the gate are rendered unreliable, and should be ignored when calculating the pulse, which is obtained from the gate according to (8). The number of unreliable points on either side of the gate, expressed with the parameter R appearing in the range of the index m, depends on the duration of the XUV pulse. As the XUV pulse duration decreases, R approaches $N_\varepsilon/2$. Therefore, we found that setting $R = N_\varepsilon/2$ works well, since it assumes the case of extremely short XUV pulses and still allows for the retrieval of longer ones.

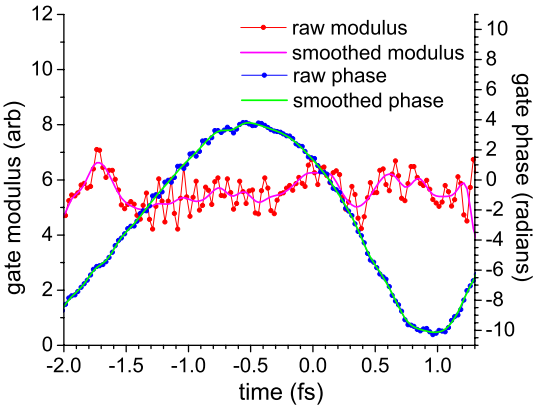

FIGURE 3 The example above shows a gate retrieved after a single iteration of the LSGPA, from the synthetic spectrogram of Fig. 4a. The initial pulse fed to the algorithm was the exact one used to construct the synthetic spectrogram, whereas the initial gate was an approximate one. After one iteration of the algorithm, the gate obtained through (9) exhibits oscillations with a period equal to four time samples. This is consistent with the delay step used for the spectrogram, which also consisted of four time samples ($L = 4$). These oscillations must be removed before applying (8), otherwise an unphysical pulse will result from the least-squares minimization step

According to (8) and (9), each gate point is calculated by using only a subset of pulse points, and each pulse point is obtained from the same subset of gate points. All in all, L subsets of the pulse and gate are obtained independently from one another following this minimization step. Each of these subsets are actually downsampled versions of the full pulse and gate, with a downsampling factor equal to L. The full pulse and gate obtained through (8) and (9) are made up of a weave of their downsampled versions, and for $L > 1$ this weave creates artifacts showing up as slight oscillations in the temporal profiles of the full pulse and gate, with a period equal to the delay step (cf. Fig. 3). Fortunately, the gate's phase and modulus oscillate at (approximately) the laser frequency, which is much smaller than the delay sampling rate. Given that the gate is accurately sampled at the delay step, the artificial oscillations can be suppressed by averaging its modulus and phase over L adjacent points, and using a cubic spline to accurately interpolate through all the gate samples. If these artifacts are removed before executing the least-squares minimization step, then the next pulse is calculated from a more physical gate, and this allows the algorithm to properly converge to a pulse and gate without these artificial oscillations. In this manner, the interpolation of the spectrogram along the delay axis during the preprocessing stage has been replaced by the dynamic interpolation of the gate at every iteration, a substantially more accurate operation.

4 Inversion of spectrograms

In this section we will establish the reliability of our algorithm by simulating attosecond streaking spectrograms with realistic experimental parameters. Attosecond

pulses are currently produced either by spectral filtering the XUV radiation [14], or by means of polarization gating [7]. Although these techniques are capable of isolating most of the power contained in a single attosecond pulse, they are not able to completely suppress the energy contained in the satellites, which are coherent and generated at every half-cycle of the laser field. An atom that is photoionized by such XUV pulses will release electron wave packets with a similar temporal structure: they will consist of a strong attosecond pulse accompanied by one or more weaker satellites mutually separated by half optical cycles of the laser field. If the ionization occurs in the presence of an IR streaking field, the spectral shifts of the resulting electron wave packets are offset by half a laser period: when the main electron wave packet is accelerated by the IR field, the adjacent satellites are decelerated.

When two or more coherent attosecond pulses ionize atoms, the interference between the electron wave packets causes the appearance of spectral fringes. The streaking field influences this interference, and thus the position of the spectral fringes changes with the delay between the XUV and IR fields. Consequently, these spectral fringes contain important information about the relative timing, intensity and phase between the wave packets, and therefore must be properly recorded. The fringe pattern in the spectrogram is easily affected by any type of defect in the acquisition process. First and foremost, a sufficient spectral resolution is necessary in order to resolve these fringes, which are spaced by the energy of two laser photons of the generating field. In the case of a 750 nm streaking pulse, this implies an energy resolution better than ~ 1.6 eV, which is easily achievable with current time-of-flight spectrometers.

Figure 4a shows a spectrogram resulting from a train of two XUV pulses separated by half an optical cycle of the streaking field. In this example, spectra were calculated at de-

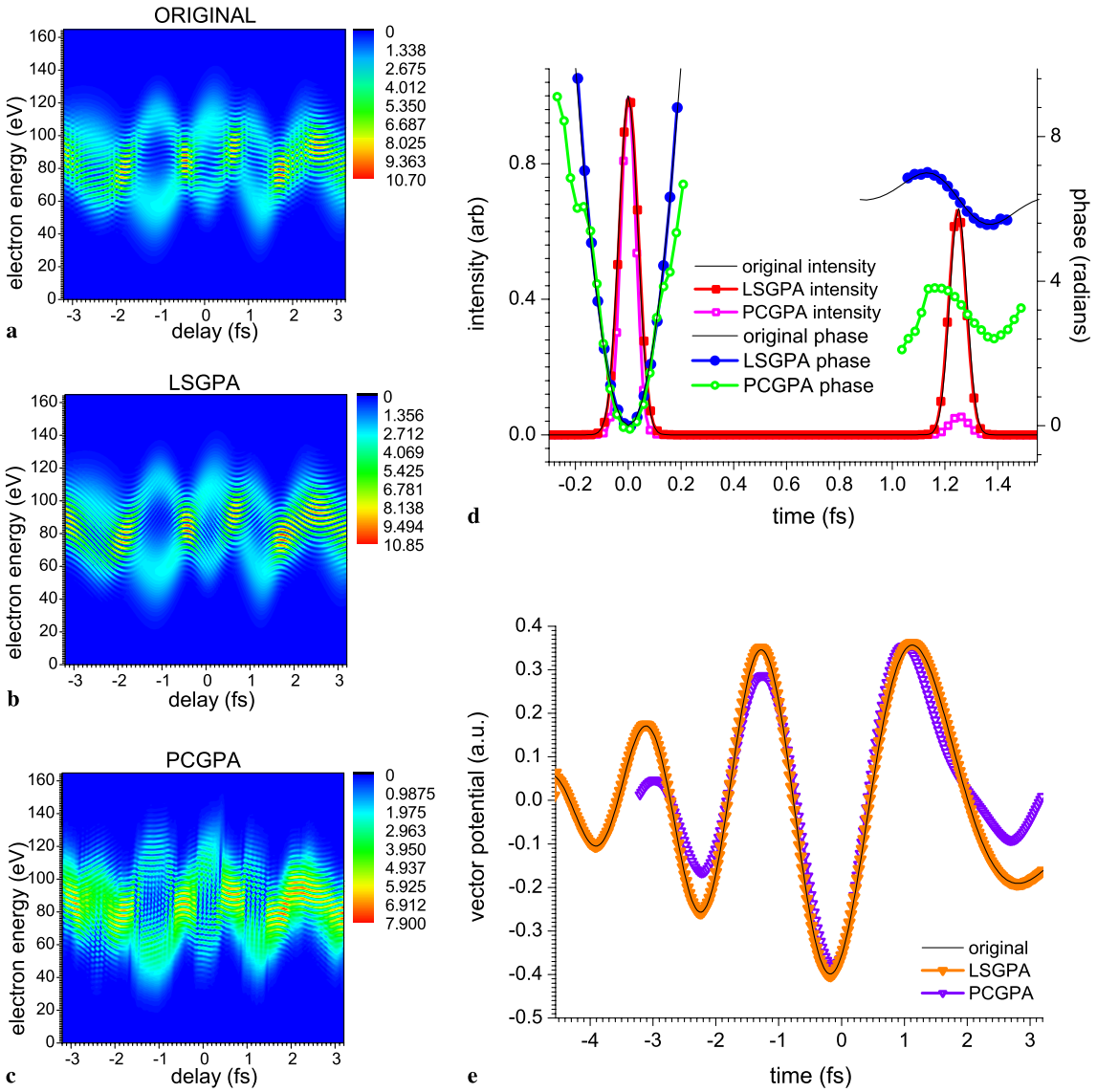

FIGURE 4 In order to compare the LSGPA to the PCGPA, an attosecond streaking spectrogram was calculated using a double pulse structure. The spectrogram in (**a**) was chosen to fall outside the PCGPA's parameter space. Namely, the delay range was chosen to be smaller than the duration of the IR streaking, so that periodic boundary conditions would not apply along the delay axis (and therefore to the gate). Additionally, a large enough delay step was used in order to confuse the fringe pattern, rendering the interpolation along the delay axis especially nefarious

lay intervals of 100 as, with an energy resolution of 0.64 eV. For simplicity, the original spectrogram fed to both algorithms was calculated using the central momentum approximation. The streaking field was modeled using a chirped Gaussian pulse with a FWHM duration of 4.0 fs, a peak intensity of 2.4×10^{13} W/cm^2, a central carrier wavelength centered at 750 nm, and a constant GDD of 2 fs^2. The XUV field consisted of a sequence of two attosecond pulses separated by a half-cycle of the IR field (1.25 fs) with a 3 : 2 peak intensity ratio. The most intense XUV pulse had a duration of 85 as, while the weaker one had a duration of 76.5 as, and both pulses were chirped as shown in Fig. 4d. The LSGPA retrieval was performed on a 256×65 grid, while the PCGPA required the spectrogram to be interpolated along the delay axis up to a size of 256×256, in order to satisfy its time-energy sampling constraint.

The checkerboard patterns of the spectrogram in Fig. 4a, which is the actual spectrogram given to the PCGPA (an interpolated version of the original one), testify that the delay step used in this example was not fine enough to resolve the smooth variation of the fringe pattern along the delay axis. As a result, the spectra resulting from the interpolation along the delay axis are not physical, as they are not the correct spectra that should appear at these delay values. The large number of unphysical spectra (three interpolated spectra for each known spectrum) precludes an accurate retrieval by the PCGPA because the interpolated spectrogram no longer conforms to definition (3), in that it can no longer be expressed in terms of a single pulse and gate pair. Surprisingly, the retrieved XUV pulses nonetheless exhibit the correct qualitative behavior, as evidenced by Fig. 4d; while Fig. 4e shows that the vector potential was also recovered relatively well, although its amplitude was underestimated. The spectrogram retrieved by the PCGPA (Fig. 4c) indicates that the weaker pulse's spectral components were not properly accounted for by the algorithm: they show up as artifacts in the retrieved spectrogram. Furthermore, these spectral components have also enticed the PCGPA to overestimate the main pulse's bandwidth, and underestimate its duration by $\sim 20\%$.

Since the LSGPA used only the known spectra, it was not fazed by interpolation errors, and was able to correctly characterize both XUV pulses and the streaking field. Figure 4b is the full spectrogram retrieved by the LSGPA, i.e., it is the spectrogram constructed from the retrieved pulse and gate assuming a delay step equal to one time sample ($L = 1$). It shows the proper behavior of the fringe pattern, which is what would have been displayed in the original spectrogram if a finer delay step, of precisely 25 as, were used. The LSGPA-retrieved spectrogram shows that the spectral position of the fringes changes rapidly at certain delays, and the 100 as delay step was clearly not fine enough to capture them. Nonetheless, the delay-dependent structure of the spectrogram is not an issue provided that no interpolation is performed along this axis. Figure 4d shows that the 65 spectra contained enough information to recover the XUV pulses. Their retrieved temporal structures agree quantitatively with the original ones, yielding FWHM durations of 85 and 76 as for the stronger and weaker pulses, respectively. The 3 : 2 intensity ratio, as well as the relative phase between the two pulses were also correctly retrieved. Figure 4e shows that the vector potential was also properly characterized, both in its amplitude and its absolute phase. Moreover, the vector potential was recovered over a larger time interval than that from the PCGPA. By its very construction, the PCGPA assumes the gate function to be defined strictly within the same temporal window as the spectrogram. However, due to the finite duration of the XUV field, the spectra located near minimal and maximal delays contain information about the gate outside of the delay range.

The retrieval shown in Fig. 4 has been performed on a synthetic spectrogram constructed according to (4), ignoring the dipole transition matrix element and using the central momentum approximation. Since the retrieval algorithm uses these same approximations to calculate the spectrogram at every iteration, it is not surprising that it converges to XUV and IR fields that are essentially the same as the original ones. In order to investigate the effects of the approximations, we gave the LSGPA a spectrogram calculated using the more accurate expression (1), using the independently calculated dipole transition matrix element of neon.[1] For this test we again chose the temporal structure of the XUV field to be composed of two attosecond pulses separated by a half-cycle of the IR field. The most intense pulse had a duration of 90 as, whereas the weaker one was more extended in time, with a complicated temporal intensity profile modulated on the attosecond time scale. The two XUV pulses had a central energy exceeding the ionization potential of neon by 100 eV, and were given phases with higher-order terms. The spectrogram was recorded with a delay step of 100 as, and an energy resolution of 0.3 eV. The IR field was modeled using a bandwidth-limited Gaussian pulse with a FWHM duration of 3.5 fs, a peak intensity of $\sim 7.5 \times 10^{12}$ W/cm^2, and a 750 nm central wavelength.

The approximations had a minimal effect on the retrieved XUV pulses (Fig. 5d) and the retrieved IR field (Fig. 5e). Particularly, the FWHM duration of the most intense XUV pulse is underestimated by $\sim 10\%$. In contrast, the relative absolute phase between the two pulses is off by as much as $\sim 90°$.

The small distortions in the retrieved XUV pulses and the large discrepancy in the relative phase between them are intimately linked to the errors made by using the central momentum approximation ($p \to p_0$). The difference between the exact phase (2) and the approximate one can be expressed as

$$\Delta\varphi(p,t) = \varphi(p,t) - \varphi(p_0,t) = (p - p_0) \int_t^\infty A_L(t')\,\mathrm{d}t' . \quad (10)$$

For the approximation to be valid, $\Delta\varphi(p,t)$ must vary minimally during the interaction with the XUV field. This condition can be written as

$$\epsilon(p) = \max_t |\Delta\varphi(p,t)| \ll \pi \quad (11)$$

for all momenta p where the electron flux is significantly intense. For a single isolated attosecond XUV pulse with a duration Δt_X, the IR vector potential is approximately linear over

[1] The dipole transition matrix element from the ground state of neon was calculated in the Hartree–Fock (HF) approximation. The continuum states were modeled as a linear combination of the s and d waves forming a frozen-core HF solution propagating in the direction of observation (courtesy of Y. Komninos).

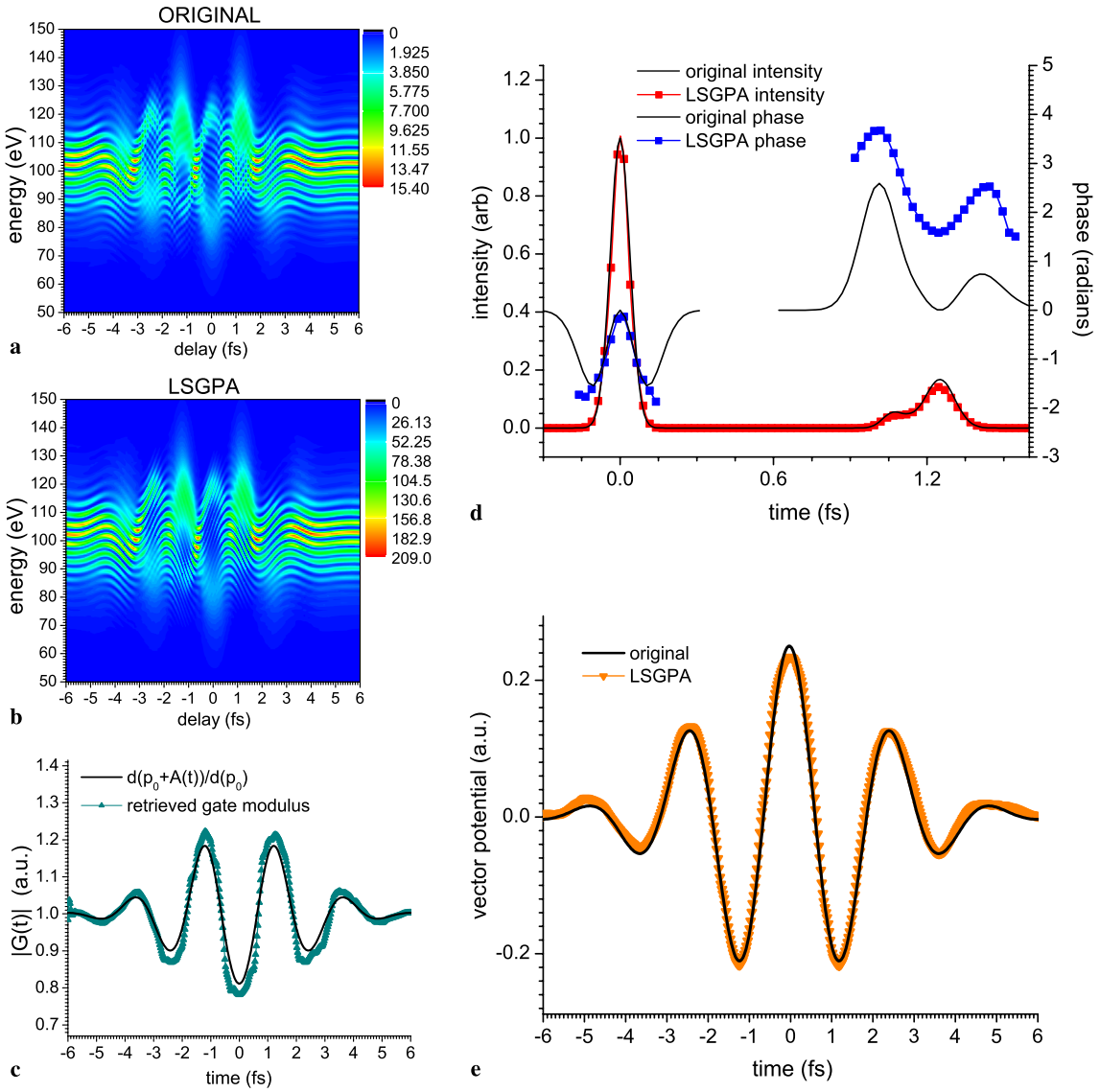

FIGURE 5 To investigate the effect of the approximations, the LSGPA was applied on a spectrogram computed without the central momentum approximation, and using the known dipole transition matrix element of neon. Before being processed with the LSGPA, the spectrogram was divided by the dipole transition matrix element of neon, according to (4). These approximations have induced slight distortions on the retrieved XUV pulse and IR vector potential, and have prevented the algorithm from retrieving the correct relative phase between the two XUV pulses

the duration of the pulse, so that the error can be estimated as

$$\epsilon_1(p) = \left| (p - p_0) \int_{t_0 - \Delta t_X/2}^{t_0 + \Delta t_X/2} A_L(t)\, dt \right| \approx \Delta t_X |(p - p_0) A_L(t_0)| , \tag{12}$$

where the XUV pulse is assumed to be centered at a moment t_0. For the simulation presented in Fig. 5, the maximum value of the vector potential is $A_{max} = 0.25$ a.u., and (12) yields an error of $\epsilon_1 \leq 0.4$ rad in the energy window between 80 and 130 eV. This small value explains why each of the XUV pulses was accurately retrieved.

The algorithm failed to recover the relative phase between the main pulse and its satellite because $\Delta\varphi(p, t)$ varied significantly over the time scale separating them. In this case, the accumulated error is

$$\epsilon_2(p) \leq \frac{2T_L}{\pi} |p - p_0| A_{max} , \tag{13}$$

where T_L is the period of laser oscillations. For the parameters used to produce Fig. 5, this error is $\epsilon_2 \leq 3.15$ radians, which is comparable to π.

The central momentum approximation also had an effect on the retrieved gate modulus, via the dipole transition matrix element. Figure 5c compares the modulus of the gate directly retrieved by the LSGPA (turquoise triangles) with its theoretical value (black line) $|G(t)| = d(p + A_L(t))/d(p) \approx d(p_0 + A_L(t))/d(p_0)$, using the original vector potential and the independently calculated dipole transition matrix element (courtesy of Y. Komninos). Although the exact gate modulus is both a function of momentum and time, by its very construction the algorithm retrieves a gate represented with a one-dimensional vector. The discrepancies between the retrieved gate mod-

ulus and its approximate theoretical (using the substitution $p \to p_0$) are a result of neglecting this momentum dependence. Nevertheless, the agreement between the two curves in Fig. 5c is evidence that the central momentum approximation applied to the dipole transition matrix element is valid. The error due to the central momentum approximation can be estimated as

$$\frac{d(p+A_{\mathrm{L}}(t))}{d(p)} - \frac{d(p_0+A_{\mathrm{L}}(t))}{d(p_0)} \approx -\left(\frac{d'(p_0)}{d(p_0)}\right)^2 (p-p_0)A_{\mathrm{L}}(t)\,. \tag{14}$$

Similarly to the phase error (12), this discrepancy is maximal at extrema of the vector potential. While at the zero crossings, where streaking broadens rather than shifts electron spectra, (4) and (5) do not suffer from the central momentum approximation. This quality can potentially be used to further improve the accuracy of FROG retrieval.

5 Conclusion

Constant improvements in technology will allow for temporally resolving physical phenomena on scales approaching the atomic unit of time (~ 24 as). Such experiments will involve the generation of XUV and electron wave packets at higher energies and shorter durations. Since our algorithm avoids interpolating the attosecond streaking spectrogram along the delay axis, it is better suited for the accurate characterization of ever shorter pulses, as long as the spectrogram is recorded within a certain range of physical parameters. Although the retrieved relative phase between the XUV pulses remains inconclusive, the attosecond FROG algorithm can correctly characterize the internal structure of the individual attosecond pulses and that of the IR vector potential, provided that the time-bandwidth product (12) is not too large. Fortunately, this requirement can be easily satisfied under realistic experimental conditions, thereby making the FROG technique a powerful and reliable tool for time-resolved measurements of attosecond physical processes.

ACKNOWLEDGEMENTS This work was supported by the DFG Cluster of Excellence: Munich-Centre for Advanced Photonics. The authors are grateful to X. Gu and F. Krausz for providing valuable insight about attosecond streaking and important discussions about the retrieval algorithm.

REFERENCES

1 M. Uiberacker, T. Uphues, M. Schultze, A.J. Verhoef, V. Yakovlev, M.F. Kling, J. Rauschenberger, N.M. Kabachnik, H. Schroder, M. Lezius, K.L. Kompa, H.G. Muller, M.J.J. Vrakking, S. Hendel, U. Kleineberg, U. Heinzmann, M. Drescher, F. Krausz, Nature **446**, 627 (2007)
2 E. Goulielmakis, M. Uiberacker, R. Kienberger, A. Baltuška, V. Yakovlev, A. Scrinzi, T. Westerwalbesloh, U. Kleineberg, U. Heinzmann, M. Drescher, F. Krausz, Science **305**, 1267 (2004)
3 R. Kienberger, E. Goulielmakis, M. Uiberacker, A. Baltuska, V. Yakovlev, F. Bammer, A. Scrinzi, T. Westerwalbesloh, U. Kleineberg, U. Heinzmann, M. Drescher, F. Krausz, Nature **427**, 817 (2004)
4 M. Drescher, M. Hentschel, R. Kienberger, M. Uiberacker, V. Yakovlev, A. Scrinizi, T. Westerwalbesloh, U. Kleineberg, U. Heinzmann, F. Krausz, Nature **419**, 803 (2002)
5 A.L. Cavalieri, N. Muller, T. Uphues, V.S. Yakovlev, A. Baltuska, B. Horvath, B. Schmidt, L. Blumel, R. Holzwarth, S. Hendel, M. Drescher, U. Kleineberg, P. M Echenique, R. Kienberger, F. Krausz, U. Heinzmann, Nature **449**, 1029 (2007)
6 Y. Mairesse, F. Quéré, Phys. Rev. A **71**, 011 401 (2005)
7 G. Sansone, E. Benedetti, F. Calegari, C. Vozzi, L. Avaldi, R. Flammini, L. Poletto, P. Villoresi, C. Altucci, R. Velotta, S. Stagira, S. De Silvestri, M. Nisoli, Science **314**, 443 (2006)
8 P.M. Paul, E.S. Toma, P. Breger, G. Mullot, F. Auge, P. Balcou, H.G. Muller, P. Agostini, Science **292**, 1689 (2001)
9 J. Itatani, F. Quéré, G.L. Yudin, M.Y. Ivanov, F. Krausz, P.B. Corkum, Phys. Rev. Lett. **88**, 173 903 (2002)
10 M. Kitzler, N. Milošević, A. Scrinzi, F. Krausz, T. Brabec, Phys. Rev. Lett. **88**, 173 904 (2002)
11 M. Lewenstein, P. Balcou, M.Y. Ivanov, A. L'Huillier, P.B. Corkum, Phys. Rev. Lett. **49**, 2117 (1994)
12 D.J. Kane, IEEE J. Quantum Electron. **QE-35**, 421 (1999)
13 R. Trebino, K.W. Delong, D.N. Fittinghoff, J.N. Sweetster, M.A. Krumbügel, B.A. Richman, Rev. Sci. Instrum. **68**, 3277 (1997)
14 M. Schultze, E. Goulielmakis, M. Uiberacker, M. Hofstetter, J. Kim, D. Kim, F. Krausz, U. Kleineberg, New J. Phys. **9**, 243 (2007)